JOC The Journal of Organic Chemistry

Article

pubs.acs.org/joc

How Does the C–Halogen Bond Break in the Photosubstitution Reaction of 3-Fluorobenzophenone in Acidic Aqueous Solutions?

Jinqing Huang,[†] Jiani Ma,*[,†,‡] Mingde Li,[†] Mingyue Liu,[†] Xiting Zhang,[†] and David Lee Phillips*[,†]

[†]Department of Chemistry, The University of Hong Kong, Pokfulam Road, Hong Kong, People's Republic of China

[‡]Key Laboratory of Synthetic and Natural Functional Molecule Chemistry of Ministry of Education, College of Chemistry and Materials Science, Northwest University, Xi'an 710127, People's Republic of China

Supporting Information

ABSTRACT: The efficient photosubstitution reaction of *m*-fluorobenzophenone and the related photohydration reactions were systematically investigated in acidic aqueous solutions. The mechanisms and intermediates were directly characterized by femtosecond transient absorption spectroscopy and nanosecond time-resolved resonance Raman spectroscopy, which is supported by density functional theory calculations. This photosubstitution was found to be a two-step process, based on the observation of a *meta*-hydration intermediate. The protonation of the ketone was confirmed as a crucial precursor step for further photochemical reactions as indicated by the observation of the absorption spectrum of an excited triplet protonated species. More interestingly, the efficient photosubstitution reaction could selectively occur under specific conditions. Control experiments on a series of halogen-substituted benzophenones were conducted to study the influence of the solution acidity, substituent positions, and the kind of substituted halogens on the efficiency in forming the corresponding hydroxyl photosubstitution product. Some practical conditions in predicting the efficiency of the photosubstitution reaction of interest are summarized, and they were successfully used to predict when the photosubstitution reaction takes place for some other halogen-substituted benzophenone derivatives. The driving force of this photosubstitution reaction may provide insights into several possible applications which are also briefly discussed.

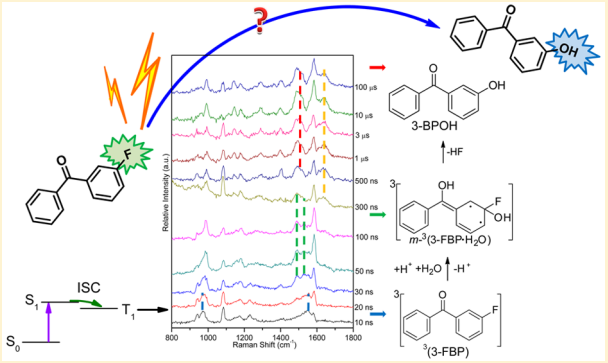

INTRODUCTION

Benzophenone (BP) and its derivatives, especially the halogen substituted ones, are widely used as photoremovable protecting groups in chemical synthesis,[1] photoactivatable groups in photolabeling for biological applications,[2−4] photoinitiators in polymerization,[5,6] and photosensitizers in some commercial applications.[7,8] The photochemical and photophysical properties of these compounds are of interest because their excited states are highly reactive in inducing electron transfer,[9,10] proton transfer,[11] hydrogen abstraction reactions,[12] and a variety of other photochemical reactions.[13−15] For the family of halogen-substituted benzophenones (BPs), different substituted halogens and different substituent positions can influence the energy gap between the lowest electronic excited states ($n\pi^*$ and $\pi\pi^*$),[16,17] leading to possible changes in their photophysical and photochemical properties, and may in some cases can lead to an efficient photosubstitution reaction.

Recent research has deepened and extended the understanding of *meta*- or *para*-halogen-substituted BP photochemical reactions.[10,18−21] Their absorption spectra have strong absorption bands, indicating increasing resonance interaction from substituents in the order of F < C1 < Br in the corresponding electronic excited states.[22] The infrared spectra of halogen-substituted BPs are comparatively complicated because the heavy halogen on the benzene ring can cause splitting features within several wavenumbers in *para*- and *meta*-substituted BPs.[23,24] Moreover, their relative electron affinities have been investigated to understand the electron transfer in some photoinduced processes. The values of 4-fluorobenzophenone (1.2 kcal/mol) and that of 4-chlorobenzophenone (3.7 kcal/mol) are indicative of the π donor abilities of the substituted halogens.[25] However, the halogen substituents can also act as electron-withdrawing groups to increase the hydrogen abstraction capability of halogenated BPs significantly.[26] Hence, the halogen substituents can be crucial in changing the nucleophilic properties for different derivatives, representing a combination of resonance and inductive effects. Recently, Wirz and co-workers reported and explained the proton quenching of the triplet species by the hydration of a triplet-protonated intermediate,[27] which is reversible for BP and its derivatives except for 3-fluorobenzophenone (3-FBP), which instead appeared to undergo an unusual and efficient photosubstitution reaction to make 3-hydroxybenzophenone.[15] Previous studies indicated that the active substituent at a *meta*-position can lead to several unusual types of photochemical

Received: June 10, 2015
Published: August 31, 2015

DOI: 10.1021/acs.joc.5b01308
J. Org. Chem. 2015, 80, 9425−9436

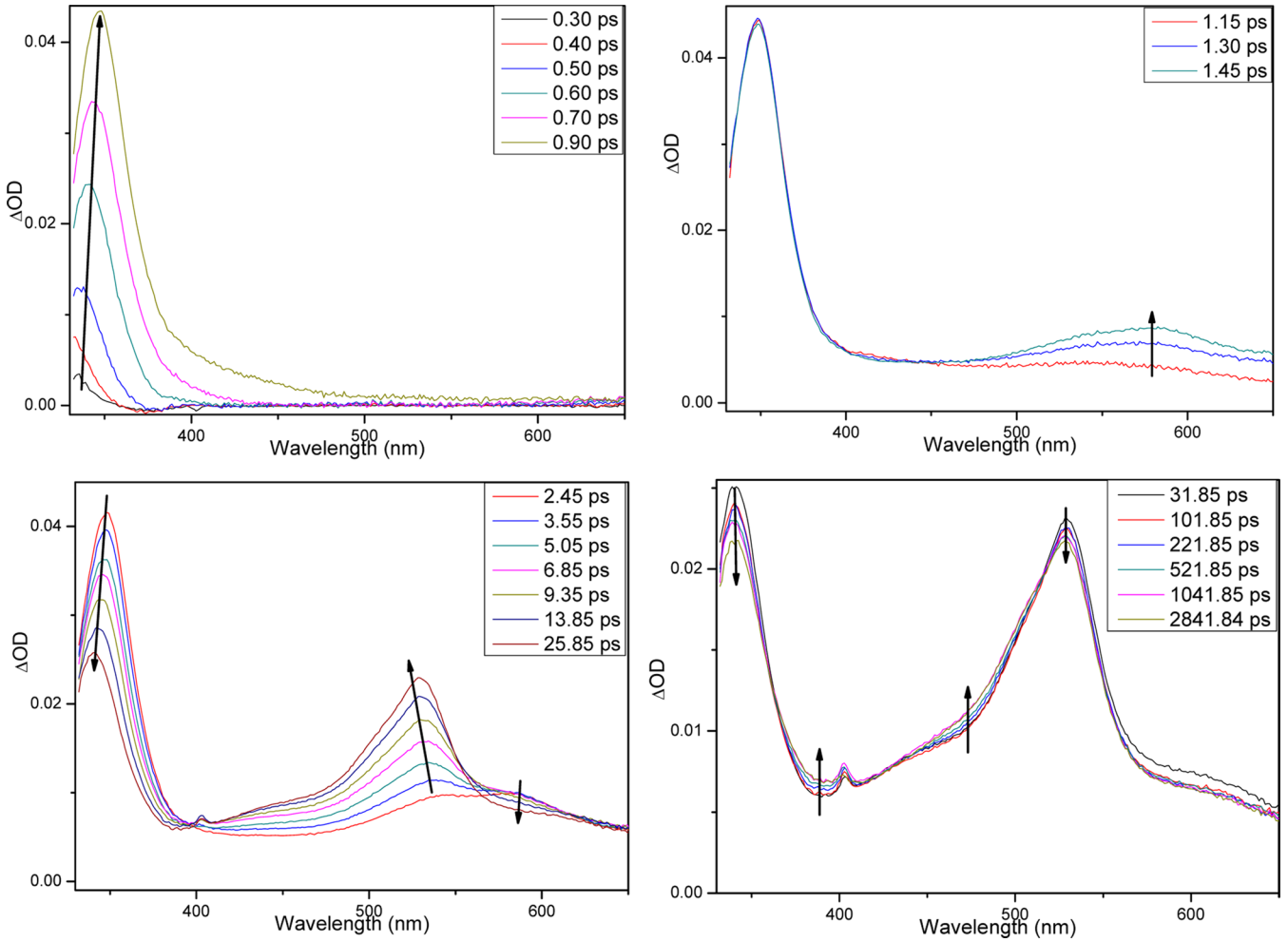

Figure 1. Fs-TA spectra of 3-BrBP in 1.00 M $HClO_4$ CH_3CN/H_2O (1:1 by volume) solution obtained after 266.6 nm excitation.

reactions.[28,29] This photosubstitution reaction of 3-FBP may be a new case. Nonetheless, a detailed mechanism remains unclear due to limited information obtained from direct observations of the reactive intermediates. Moreover, it is reasonable to expect similar substitution reactions may also occur for other halogen-substituted BPs according to the basic principles of organic chemistry,[30,31] but to our knowledge, there are as yet no such photosubstitution reactions reported for other halogen analogues.[27] Further in-depth studies on the different substituent positions and different substituted halogens on BP derivatives may provide a possible interpretation for this puzzling phenomenon.[32,33] However, a relatively satisfactory explanation has not come forth due to the complicated influences from various external and internal factors on this photosubstitution reaction.

Since our previous studies have elucidated the substituent position effect on C−H activation of *m*- and *p*-methylbenzophenones by employing a systematic time-resolved spectroscopic investigation,[29] time-resolved spectroscopic experiments and theoretical computations are combined to gain more insight into how the 3-FBP photosubstitution can occur and when it may be able to occur for other halogen-substituted BP systems.[34,35] The femtosecond transient absorption (fs-TA) and nanosecond time-resolved resonance Raman (ns-TR^3) spectroscopic experiments are adopted to directly detect the conversions of the electronic excited states and the transformations of intermediates associated with several halogen-substituted BPs. Density functional theory (DFT) simulations were also performed to help analyze the experimental results. Furthermore, the driving force behind this photosubstitution reaction is discussed by comparing the photoinduced reactions of these halogen-substituted BPs under different acidic conditions, between different substituent positions, and among different substituted halogens. The factors influencing the photosubstitution reaction are examined to extend the understanding of the interesting "meta effect"[29] and "heavy atom effect"[36] phenomena observed in the photophysics and photochemistry of BP derivatives. Several possible mechanisms are briefly discussed, including halogen elimination reactions through an excited-state intramolecular proton-transfer model as well as the position of halogen attachment on the phenyl rings of BP in relation to the selectivity for aromatic substitution reactions. These new results provide significant insight into the decomposition of halogenated BPs in aqueous solutions and may be useful for future investigations of related reactions in aqueous environments and in designing methods to minimize the impact of environmental pollution related to the aromatic halogen compounds. Other possible applications such as a new photochemical synthetic methodology for halogen elimination or hydroxyl substitution and a novel way to change the photophysical and photochemical properties of photosensitive materials by halogen substituent modification very likely will be established by other researchers in the future.

DOI: 10.1021/acs.joc.5b01308
J. Org. Chem. 2015, 80, 9425−9436

RESULTS AND DISCUSSION

A. Mechanism of the Photosubstitution Reaction of *m*-Fluorobenzophenones. The photophysical and photochemical properties of halogen-substituted BPs were investigated by time-resolved spectroscopic methods in an inert organic solvent, a strong hydrogen donor solvent, and an aqueous solution. As a representative example, the fs-TA, nanosecond time-resolved transient absorption (ns-TA), and ns-TR^3 results for 3-FBP in CH_3CN, 2-propanol, and CH_3CN/H_2O (1:1 by volume) solution are presented in the Supporting Information (Figures 2S−12S). The behaviors of 3-FBP and other halogen-substituted BPs strongly resemble their parent compound BP.[37] This indicates that the halogen substituent at the *meta*- or *para*-position does not exert much influence on the photophysics and photoreduction reaction of the BP derivatives in the inert organic solvent, the strong hydrogen donor solvent, and the mixed neutral aqueous solution.

In 1.00 M $HClO_4$ CH_3CN/H_2O (1:1 by volume) solution, the fs-TA spectra of 3-bromobenzophenone (3-BrBP) are similar to the spectra obtained in CH_3CN in Figure 13S except the last profile. As shown in Figure 1, the short wavelength absorption band gradually increased at 340 nm in the first profile, and then a less intense band appeared at around 570 nm in the second profile. The global analysis of the first and second processes yields the time constants of 7.6 and 0.4 ps, respectively. (See the Supporting Information, Figure 14S, for details.) On the basis of the previous study of BP,[27] the first and second profiles indicate early photoinduced processes: The ground state of 3-BrBP was transferred to a higher excited singlet state S_n and then went through an internal conversion (IC) to the first singlet excited state S_1. In the third profile, a broad band at 530 nm grew while the 340 nm band decreased in intensity. The clear isosbestic point at 390 nm suggests a dynamic conversion between two species and is assigned as the intersystem crossing (ISC) from S_1 to the triplet excited state T_1. The time constant obtained from global kinetic analysis in Figure 14S is 26.1 ps, which is consistent with previous experimental observations on BP.[27] In the last profile, the isosbestic points at 360, 440, and 515 nm indicate a dynamic conversion from T_1 to other species that has a broad band from 330 to 400 nm and another band at around 500 nm. The above kinetic discussions are in accordance with the time constants for the temporal dependence of the absorbance at 527 nm by a kinetics fitting using a three exponential function shown in Figure 15S. Since it has been well documented that aromatic ketones become more basic in their excited state in comparison to their ground state,[27] the formation of protonated 3-BrBP (^{3}(3-BrBP·H$^+$)) is likely responsible for the quenching of T_1, similar to analogous reactions of BP[27] and 3-methylbenzophenone[29] in acidic aqueous solutions. The pK_a of the triplet excited state of protonated BP was determined to be −0.4 ± 0.1 by Wirz and co-workers,[27] and it is reasonable to estimate a similar value for these halogen-substituted BPs. Hence, the existence of ^{3}(3-BrBP·H$^+$) in 1.00 M $HClO_4$ conditions is unfavorable in a chemical equilibrium. Moreover, protonation is the rate-determining step that leads to further chemical reactions; thus, the detection of ^{3}(3-BrBP·H$^+$) is kinetically difficult in a moderately concentrated aqueous solutions. However, the formation of the triplet protonated species may not be neglected in the photochemistry of other *meta*- or *para*-halogen-substituted BPs in acidic aqueous solutions, even if the signal is indistinctive in Figure 16S.

Figure 2 displays the ns-TR^3 spectra of 3.0 × 10^{-3} M 3-FBP in 1.00 M $HClO_4$ CH_3CN/H_2O (1:1 by volume) solution

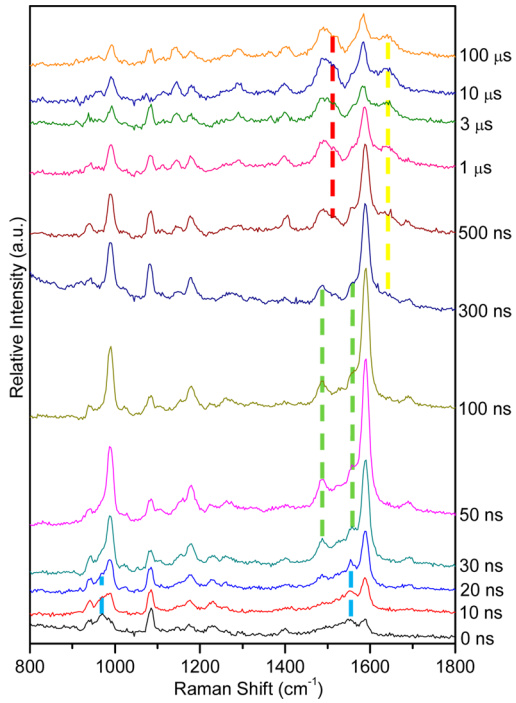

Figure 2. Ns-TR^3 spectra of 3.0 × 10^{-3} M 3-FBP in 1.00 M $HClO_4$ CH_3CN/H_2O (1:1 by volume) solution obtained after 266.0 nm excitation with a probe wavelength of 319.9 nm.

obtained after 266.0 nm excitation with a probe wavelength of 319.9 nm. The first species observed (marked with blue dashed lines) is assigned as the triplet excited-state species ^{3}(3-FBP) from a comparison to ns-TR^3 spectra obtained in CH_3CN (see Figure 18S, Supporting Information). As ^{3}(3-FBP) is quenched, a new species (marked with green dashed lines) is generated with a characteristic Raman band at 1488 cm^{-1}. Later, a third species (marked with a yellow dashed line) is observed with a representative band at 1641 cm^{-1}. Finally, a fourth species (marked with a red dashed line) is detected. To clarify the TR^3 spectra of the new species as well as their kinetics, the contribution of the ketyl radical intermediate is removed by subtracting an appropriately scaled Raman spectrum obtained in 2-propanol at 100 ns using the criterion of the Raman features at ∼1600 and 1693 cm^{-1} (see the subtraction process displayed in Figure 18S). In Figure 3, the subtracted spectra of the second new species show distinct Raman bands at 987, 1154, 1185, 1259, 1296, 1488, 1528, and 1585 cm^{-1}, similar to the Raman spectra of the triplet state of the hydration species of BP at the *meta*-position observed in our previous study.[38] Hence, it is reasonable to assign the second species as the triplet state of the hydration species of 3-FBP at the *meta*-position, denoted as *m*-^{3}(3-FBP·H_2O). This assignment is well supported by good agreement between the experimental Raman spectrum vibrational frequency pattern with the respective calculated Raman spectrum of *m*-^{3}(3-FBP·H_2O). Similarly, the third species is assigned as the singlet state of the hydration species of 3-FBP at the *ortho*-position, denoted as *o*-^{1}(3-FBP·H_2O), according to the photohydration reaction of BP in acidic aqueous solutions.[22] The experimental Raman spectrum is compared with the simulated Raman spectrum of

DOI: 10.1021/acs.joc.5b01308
J. Org. Chem. 2015, 80, 9425−9436

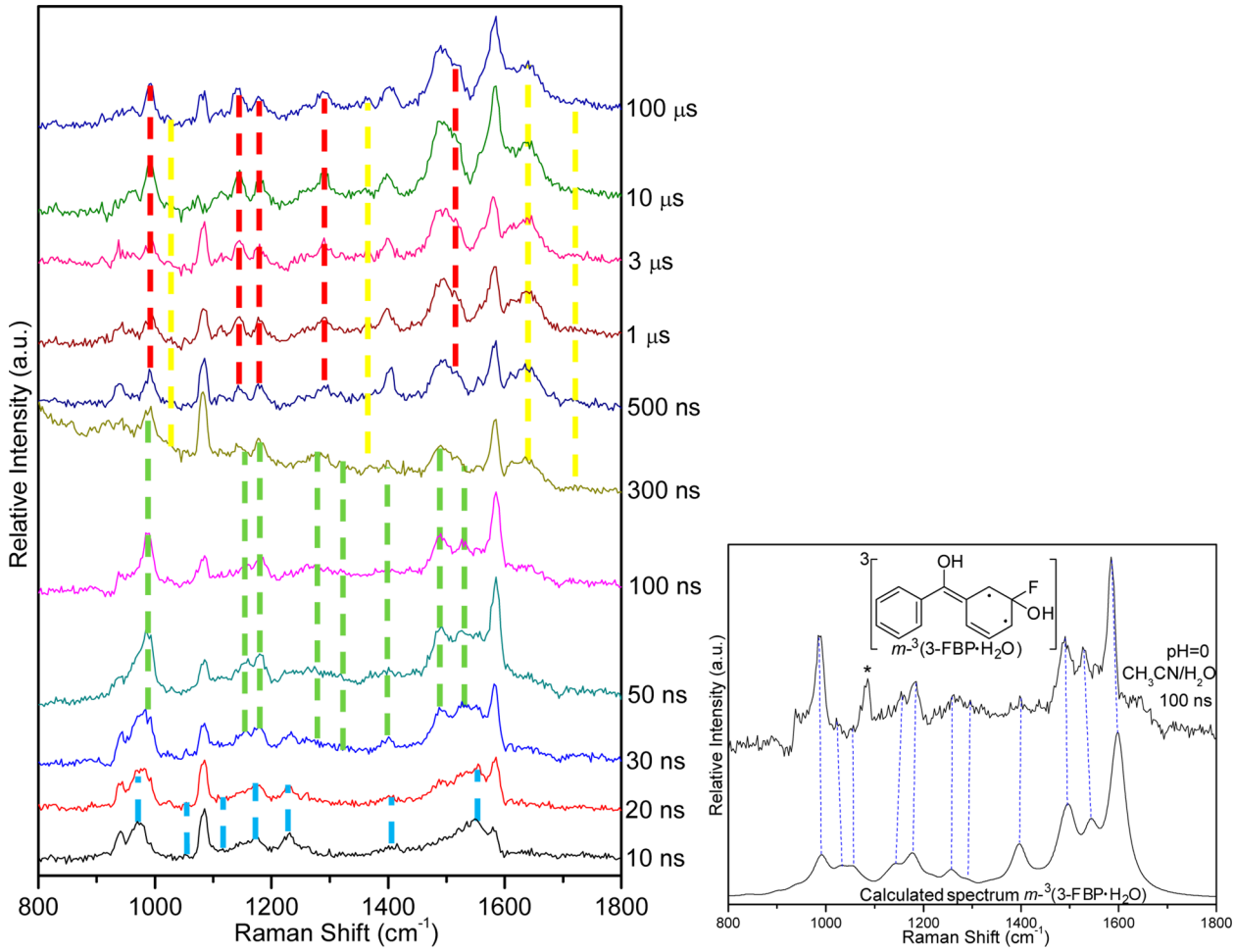

Figure 3. (Left) Subtracted ns-TR^3 spectra of 3.0×10^{-3} M 3-FBP in 1.00 M $HClO_4$ CH_3CN/H_2O (1:1 by volume) solution where the contribution from the ketyl radical intermediate and solvent have been removed. (Right) A comparison of a representative subtracted Raman spectrum recorded at 100 ns in a 1.00 M $HClO_4$ CH_3CN/H_2O (1:1 by volume) solution and the DFT-calculated Raman spectrum of m-^{3}(3-FBP·H_2O).

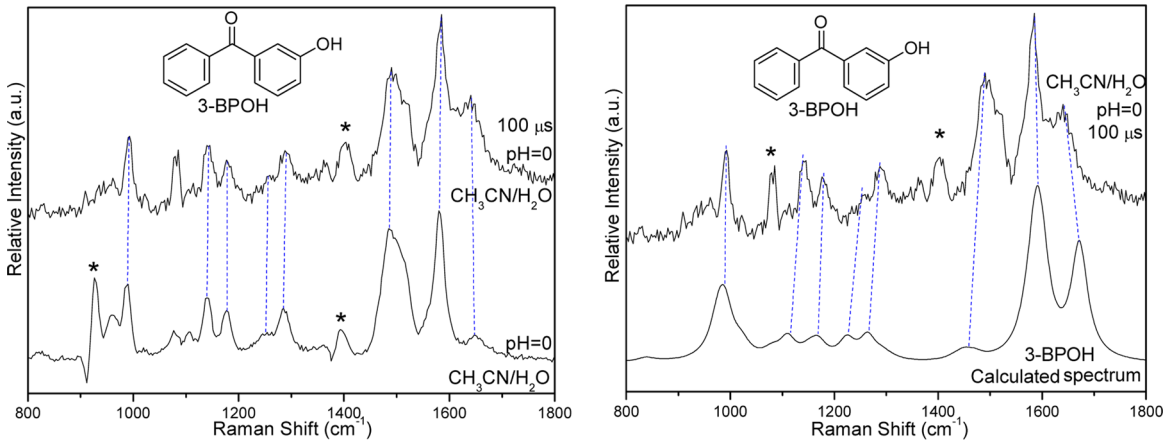

Figure 4. (Left) Comparison of the Raman spectrum recorded at 100 μs in 1.00 M $HClO_4$ CH_3CN/H_2O (1:1 by volume) solution and the Raman spectrum of commercial chemical 3-BPOH obtained by a probe wavelength of 319.9 nm. (Right) Comparison of the Raman spectrum recorded at 100 μs in a 1.00 M $HClO_4$ CH_3CN/H_2O (1:1 by volume) solution and the DFT-calculated Raman spectrum of 3-BPOH.

o-^{1}(3-FBP·H_2O) in Figure 19S to validate this speculation. The last species, which is the final product, remains stable up to 100 μs and has Raman bands at 993, 1139, 1176, 1287, 1490, 1589, and 1651 cm^{-1}. These Raman features are essentially identical to our control experiment using an authentic sample of pure 3-hydroxybenzophenone (3-BPOH) under the same conditions. In Figure 4, the experimental Raman spectrum at 100 μs matches well with our computational results performed on 3-BPOH, and the band observed at 1490 cm^{-1} corresponds to the OH-bending mode. This provides further support for the assignment of the final product as well as a previous report on the formation of the corresponding m-hydroxy-substituted BP

DOI: 10.1021/acs.joc.5b01308
J. Org. Chem. 2015, 80, 9425−9436

Scheme 1. Proposed Reaction Mechanism of 3-FBP in Acidic Aqueous Solutions

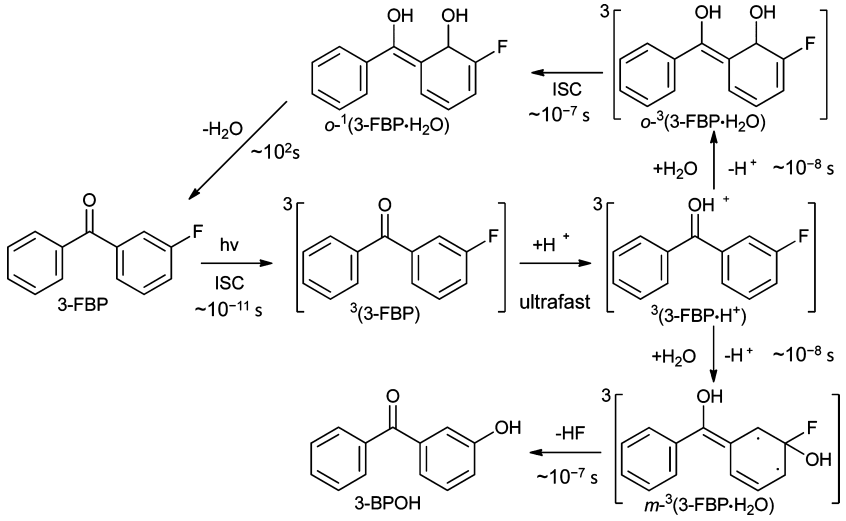

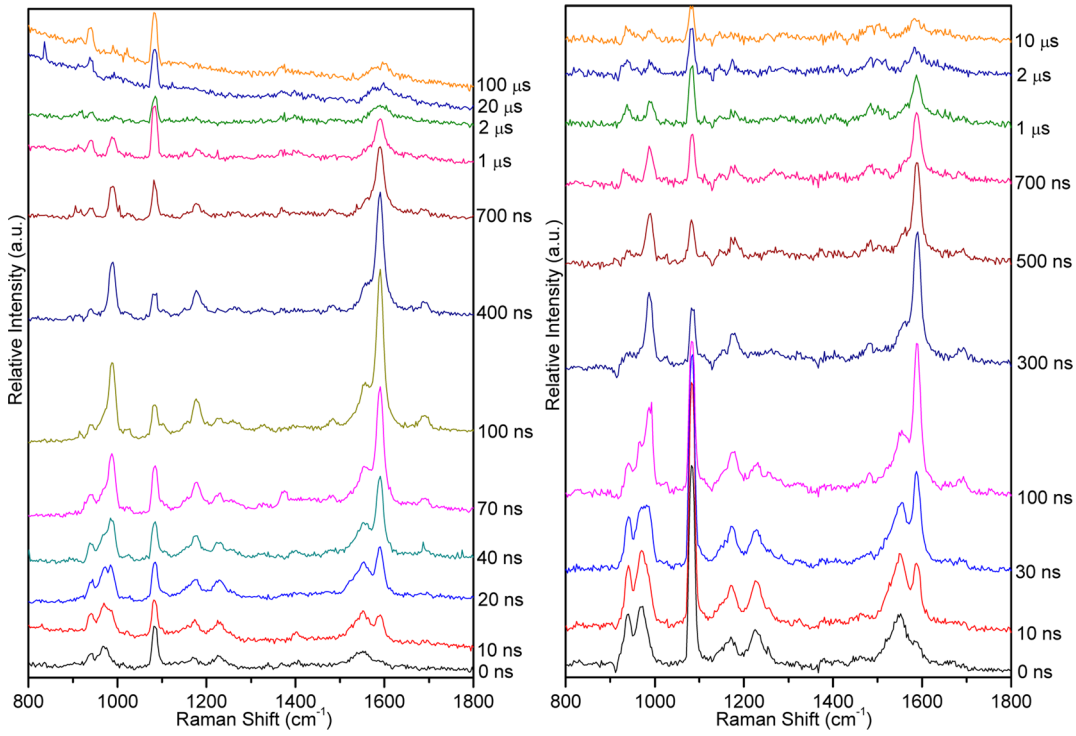

Figure 5. (Left) ns-TR^3 spectra of 3.0×10^{-3} M 3-FBP in 0.01 M $HClO_4$ CH_3CN/H_2O (1:1 by volume) solution obtained after 266.0 nm excitation with a probe wavelength of 319.9 nm. (Right) ns-TR^3 spectra of 3.0×10^{-3} M 3-FBP in 0.10 M $HClO_4$ CH_3CN/H_2O (1:1 by volume) solution obtained after 266.0 nm excitation with a probe wavelength of 319.9 nm.

derivative in the photosubstitution reaction reported by Wirz and co-workers.[27] When the fs-TA and ns-TR^3 results are combined, a summary of the major photoinduced process of 3-FBP is presented in Scheme 1: Upon irradiation, 3-FBP underwent an ISC process to form ^{3}(3-FBP), which was then protonated at the carbonyl oxygen to produce the transient species ^{3}(3-FBP·H$^+$). Consequently, the hydration reaction took place on the *meta*- or the *ortho*-positions to form the hydration species *m*-^{3}(3-FBP·H_2O) and *o*-^{1}(3-FBP·H_2O), respectively. The leaving of HF from the *meta*-hydration species resulted in 3-BPOH, where the photosubstitution reaction occurred. The leaving of water from the *ortho*-hydration species led to production of the original 3-FBP.

Similar investigations were performed for 3,3′-difluorobenzophenone (3,3′-DFBP) to confirm the proposed mechanism of the photosubstitution reaction in acidic aqueous solutions. In Figure 21S, the ns-TR^3 spectra of 3.0×10^{-3} M 3,3′-DFBP in 1.00 M $HClO_4$ CH_3CN/H_2O (1:1 by volume) solution display characteristic Raman bands for the triplet state intermediate and the hydration species at the *meta*- and the *ortho*-positions. As expected, we obtained Raman spectra of the corresponding hydroxy-substituted BP at both *meta*-positions, 3,3′-hydroxybenzophenone (3,3′-BPOH). The Raman spectrum of 3,3′-DFBP recorded at 100 μs demonstrates a strong Raman peak at ~1490 cm^{-1} relating to the OH bending mode in Figure 22S. These observations further support the occurrence of the

DOI: 10.1021/acs.joc.5b01308
J. Org. Chem. 2015, 80, 9425−9436

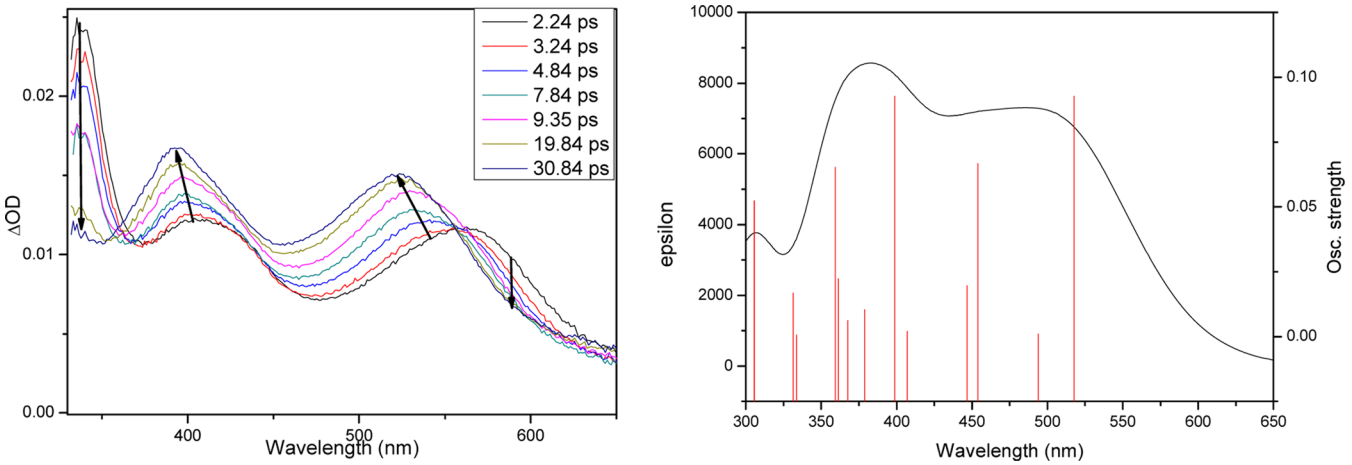

Figure 6. (Left) fs-TA spectra of BP in 5.8 M $HClO_4$ CH_3CN/H_2O (1:1 by volume) solution obtained upon 266.6 nm excitation. (Right) Simulated absorption spectrum of $^3(BP{\cdot}H^+)$ obtained from TD-DFT calculation at the B3LYP/6-311G** level of theory.

photosubstitution reaction at the fluorine-substituted positions. The proposed two-step substitution mechanism is reasonable for other *meta*-fluoro-substituted derivatives and most likely can be extended to many kinds of halogenated aromatic carbonyl systems.

B. Effect of Acidity. In order to study the effect of acidity on this photosubstitution reaction, we lowered the acidity to 0.10 and 0.01 M $HClO_4$ CH_3CN/H_2O (1:1 by volume) solutions, as shown in Figure 5. The ns-TR^3 spectra of 3.0×10^{-3} M 3-FBP in 0.10 and 0.01 M $HClO_4$ CH_3CN/H_2O (1:1 by volume) solution present characteristic Raman bands similar to that obtained in 1.00 M $HClO_4$ CH_3CN/H_2O (1:1 by volume) solution. However, the intensity of the Raman band decreases dramatically from 1.00 to 0.10 M and even further upon reaching 0.01 M. The typical Raman bands for the hydration species *m*-$^3(3\text{-FBP}{\cdot}H_2O)$ at 1488, 1528, and 1585 cm^{-1} diminish from 0.10 to 0.01 M, as is the case with another hydration species *o*-$^1(3\text{-FBP}{\cdot}H_2O)$ with a characteristic Raman band at 1641 cm^{-1}. In addition, the significant Raman band at 1490 cm^{-1} from 3-BPOH is only slightly observable in the 0.10 M solution but vanishes in the 0.01 M solution. As the acidity was decreased, the intensities of the typical Raman bands appear reduced following the same trend, indicating a high correlation between the hydration reactions and the photosubstitution reaction. According to the sequence of these reactions, it is suggested that the hydration species *m*-$^3(3\text{-FBP}{\cdot}H_2O)$ is a necessary precursor to produce 3-BPOH. Furthermore, by raising the acidity, the intensity of the Raman bands become enhanced significantly, indicating an increase of the reaction efficiency. Therefore, both the hydration reaction and the photosubstitution reaction are catalyzed by acid, which is similar to related reactions for its parent compound BP.[27]

To further investigate the acid-catalysis mechanism, we conducted fs-TA experiments for BP and 3-FBP in an extremely acidic solution (5.8 M $HClO_4$). Since this proton concentration is between the pK_a for the triplet excited state of protonated BP (−0.4) and the pK_a for the ground state of protonated BP (−4.7),[22] the triplet protonated BP ($^3(BP{\cdot}H^+)$) is readily detectable. Besides, this proton concentration is a little lower than the pK_a for the singlet excited state of protonated BP (−1.0), which could avoid the protonation in the singlet excited state. Figure 6 demonstrates the dynamic conversion between two species with clear isosbestic points at 370 and 560 nm to generate a species with two bands at 390 and 520 nm. This species is assigned as $^3(BP{\cdot}H^+)$ according to the good agreement between the experimental spectrum and the simulated spectrum in Figure 6. The following fs-TA spectra indicate the decay of $^3(BP{\cdot}H^+)$ and the formation of two hydration species in Figure 23S, supported by the TD-DFT computations in Table 1S. Since the protonation of the ground-state molecule is negligible in 5.8 M $HClO_4$ solution, this photoinduced process began from the unprotonated species. The unprotonated singlet state interconverted to the protonated triplet state through the unprotonated triplet and then went into the hydration pathways. The analogous fs-TA spectra of 3-FBP in Figure 24S indicate similar excited-state proton transfer (ESPT), i.e., $^3(3\text{-FBP}) + H^+ \rightarrow {}^3(3\text{FBP}{\cdot}H^+)$. The signal of $^3(3\text{-FBP})$ observed in the early time in ns-TR^3 is another piece of evidence to support the unprotonated triplet species in this ESPT process. Clearly, the triplet state of the protonated species is generated with the assistance of the proton provided by the acid, and it is a crucial precursor to initiate both the hydration reaction and the photosubstitution reaction. Hence, acids can promote the ESPT efficiency and facilitate the whole photochemical process.

Furthermore, the photoinduced process in the 1.00 M $HClO_4$ solution starting from the neutral ground-state molecule indicates the lowest n,π^* state instead of the π,π^* state as the major excitation character. For halogenated BPs, the electron-withdrawing capacity from the substituted halogen could enhance the contribution to the reactive n,π^* state, promoting the triplet quantum yields and the photochemical reactivity.[39] The schematic diagrams depicting the electron density for the LUMO and HOMO of $^3(3\text{-FBP}{\cdot}H^+)$ are shown in Figure 25S, providing significant configurations of π electron density. The low electron density on the *meta*-position attracts the addition of water molecules and stabilizes the *meta*-hydration species, promoting the subsequent substitution reaction. Therefore, the photosubstitution reaction and the related hydration reactions are enhanced by the halogen substituent.

C. Effect of Substituent Position. Some comparison studies were carried out for 4-fluorobenzophenone (4-FBP) to reveal the effect of the substitution position. The photophysical and photochemical properties of 4-FBP in CH_3CN, 2-propanol, and CH_3CN/H_2O (1:1 by volume) solution are the same as 3-FBP under the same conditions, demonstrated by results from fs-TA and TR^3 experiments in Figures 26S−29S. However, the

DOI: 10.1021/acs.joc.5b01308
J. Org. Chem. 2015, 80, 9425−9436

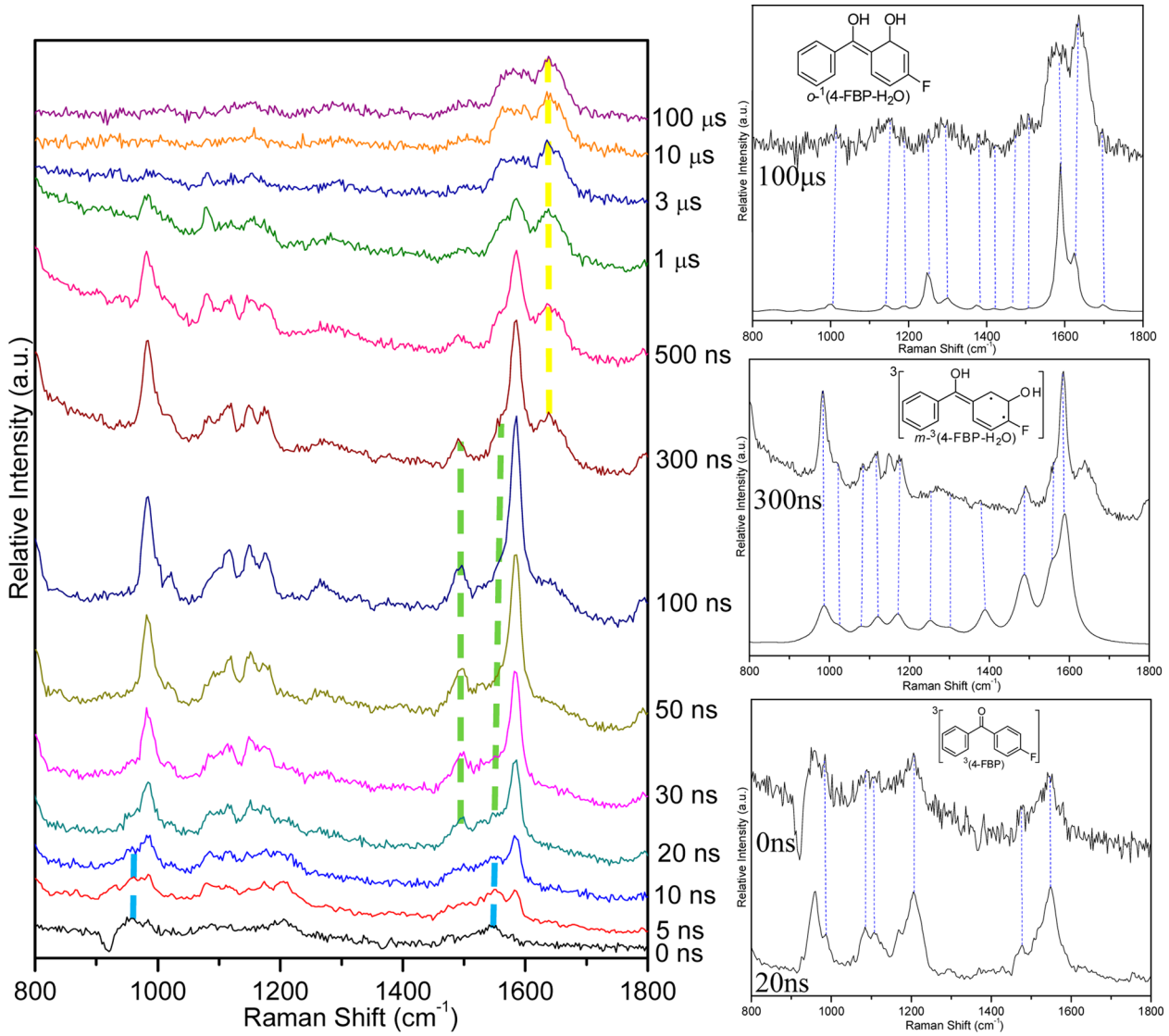

Figure 7. (Left) Ns-TR^3 spectra of 3.0×10^{-3} M 4-FBP in 1.00 M $HClO_4$ CH_3CN/H_2O (1:1 by volume) solution obtained after 266.0 nm excitation with a probe wavelength of 319.9 nm. (Right) Comparisons between the Raman spectra of 4-FBP recorded at 0, 300, and 100 μs in 1.00 M $HClO_4$ CH_3CN/H_2O (1:1 by volume) solution and the DFT-calculated Raman spectra for o-^{1}(4-FBP-H_2O), m-^{3}(4-FBP-H_2O), and 4-FBP in CH_3CN at 20 ns.

ns-TR^3 spectra present a different result in the 1.00 M $HClO_4$ solution. In Figure 7 (left), the first species observed (marked with blue dashed lines) is assigned as the triplet excited-state species ^{3}(4-FBP) from a comparison to ns-TR^3 spectra obtained in CH_3CN at 20 ns from Figure 27S. The second new species with Raman bands at 1497, 1527, and 1585 cm^{-1} is assigned as the triplet state of the hydration species of 4-FBP at the *meta*-position, denoted as m-^{3}(4-FBP·H_2O). Similarly, the third species with significant broad Raman bands at 1585 and 1638 cm^{-1} is assigned as the singlet state of the hydration species of 4-FBP at the *ortho*-position, denoted as o-^{1}(4-FBP·H_2O). These assignments are supported by good agreements in the vibrational frequency patterns between the simulated Raman spectra and the experimental Raman spectra shown in Figure 7 (right). However, no substituted product is detected in 4-FBP in the 1.00 M $HClO_4$ CH_3CN/H_2O (1:1 by volume) solution. Since the hydration reaction only occurred at the *meta*- and the *ortho*-positions while the fluorine is substituted at the *para*-position, there is no chance to produce a hydration species with the leaving fluorine and the attacking hydroxyl attached to the same aliphatic carbon center. In addition, the C−F bond is strong enough to avoid the formation of a carbocation intermediate by the leaving of the substituted fluorine, which excludes the possibility of the S_N1 substitution reaction mechanism.

It is obvious that the hydration reaction took place at the *ortho*- and the *meta*-positions selectively. To investigate the effect of substituent position, the DFT calculations for the hydration reactions of 3-FBP were performed to obtain the optimized geometries presented in Figure 30S. The energy barriers for the hydration reactions at the *meta*-, *ortho*-, and *para*-positions are 2.3, 6.4, and 7.1 kcal/mol, respectively. Comparison between the activation barriers indicates that the *meta*-position is the most favorable and the *ortho*-position is less preferred. Table 2S (Supporting Information) lists the sum of the electronic and thermal free energies for all three kinds of hydration species in both the triplet and singlet states. m-^{3}(3-FBP·H_2O) and o-^{1}(3-FBP·H_2O) have relative low energy, and

DOI: 10.1021/acs.joc.5b01308
J. Org. Chem. 2015, 80, 9425−9436

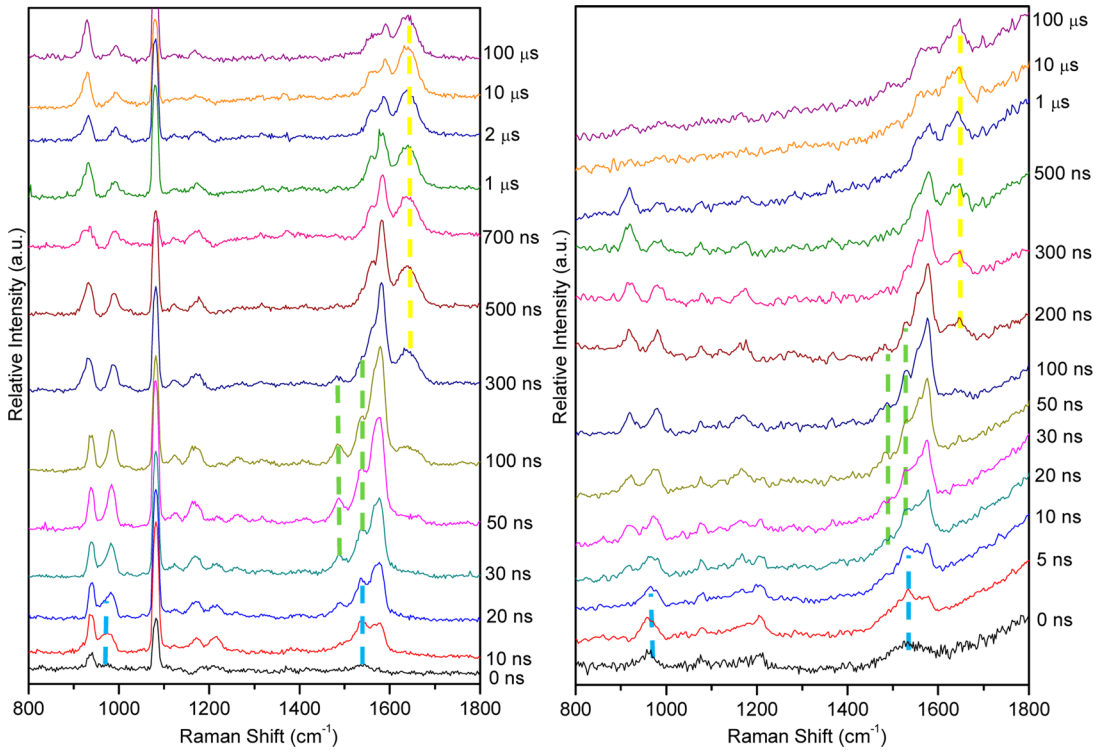

Figure 8. (Left) ns-TR^3 spectra of 3.0×10^{-3} M 3-ClBP in 1.00 M $HClO_4$ CH_3CN/H_2O (1:1 by volume) solution obtained after 266.0 nm excitation with a probe wavelength of 319.9 nm. (Right) ns-TR^3 spectra of 3.0×10^{-3} M 3-BrBP in 1.00 M $HClO_4$ CH_3CN/H_2O (1:1 by volume) solution obtained after 266.0 nm excitation with a probe wavelength of 319.9 nm.

these two intermediates can be probed by ns-TR^3 spectroscopy. To summarize the theoretical studies on 3-FBP, the hydration reaction is both kinetically and thermodynamically feasible at both the *meta*- and the *ortho*-positions, and especially at the *meta*- position. Moreover, this interesting *meta* effect is consolidated by the reorganization of the charge distribution in the benzyl derivatives upon radiation. The accumulation of excess charge during the HOMO−LUMO excitation is found predominantly in the *meta*-position and, to a lesser extent, in the *ortho*-position, and it is enhanced by the electronegativity of the *meta*-substituted fluorine. The protonated species ^{3}(3-FBP·H^+) with a positive charge located at the *meta*-position is not stable in polar solvents, promoting the hydration reaction by forming the more stable intermediate which eventually results in a heterolytic cleavage of the leaving group. Additionally, this *meta* effect is further supported by *m*-methyl activation for 3-methylbenzophenone, 3-hydroxybenzophenone, and 2-(1-hydroxyethyl)-9,10-anthroquinone.[28,29] According to our previous studies on similar compounds and the results for the halogen-substituted BPs here, the *meta*-effect gives rise to a novel and very efficient photochemistry such as photoredox reactions and photosubstitution reactions.[16]

D. Effect of Substituted Halogen. We then investigated the effect of the kind of substituted halogen in these systems. The control experiments were performed on 3-chlorobenzophenone (3-ClBP) and 3-BrBP under the same conditions. The fs-TA spectra and ns-TR^3 spectra are similar to those of 3-FBP in CH_3CN, 2-propanol, and CH_3CN/H_2O solution and indicate the same photochemistry processes occur on similar time scales. Nevertheless, the signal of 3-BPOH is absent in the ns-TR^3 spectra for either 3-ClBP or 3-BrBP in 1.00 M $HClO_4$ CH_3CN/H_2O (1:1 by volume) solution. In Figure 8, the first species is marked with blue dashed lines and assigned as the triplet excited state species. On the basis of assignments of other halogen-substituted BPs, the second species (marked in green dashed lines) and the third species (marked in yellow dashed lines) are verified as the triplet state of the hydration species at the *meta*-position and the singlet state of the hydration species at the *ortho*-position, respectively. The comparison between the simulated Raman spectrum and the experimental results is exhibited in Figure 31S for verification. Furthermore, it is worth noting that the characteristic Raman band at around 1641 cm^{-1} in the ns-TR^3 spectrum of 3-ClBP is much stronger than that of 3-FBP. The intensity of the Raman band at around 1641 cm^{-1} in the spectrum of 3-BrBP is also stronger than that of 3-FBP. That means the formation of the hydration species at the *ortho*-position is promoted by changing the substituted halogen from fluorine to chlorine and bromine. The Raman signals at 1488, 1528, and 1585 cm^{-1} are weak, suggesting that the insertion of the hydroxyl at the *meta*-position in the hydration reaction becomes difficult to take place. Since the Cl and Br atoms are much larger than the F atom, the hydration reaction at the *meta*-position may possibly to some degree be less favorable due to the influence of steric hindrance. Furthermore, the strong electronegativity of F decreases the electron density on the *meta*-position of FBP to attract the nucleophile, while the electronegativities of Cl and Br are weaker than that of F. In addition, the overlap of the molecular orbital from Cl and Br induces the electrons to the *meta*-position. Consequently, the nucleophile prefers to attack the unhindered position to form the hydration species at the *ortho*-position. Hence, it is unlikely to generate a stable intermediate with the leaving halide and the nucleophile attached to the same carbon center. As a result, the photosubstitution reaction is blocked, which is consistent with a proposed two-step substitution reaction mechanism.

DOI: 10.1021/acs.joc.5b01308
J. Org. Chem. 2015, 80, 9425−9436

In contrast to the photoinduced processes of 3-ClBP and 3-BrBP, the nucleophilic hydroxyl attacked the *meta*-position of 3-FBP to produce *m*-^{3}(3-FBP·H_2O) in a hydration reaction. The separation of HF in the following step indicated the photosubstitution reaction of 3-FBP is dynamically favorable. The complicated stereoelectronic effect and possible steric effect as well as the thermodynamics for the whole photochemical process of 3-FBP were investigated using computational chemistry. The reaction energy profile obtained from DFT calculations for the photosubstitution reaction of 3-FBP with the assistance of two water molecules are shown in Figure 9. The activation barrier of the hydration reaction on the *meta*-position is 2.3 kcal/mol and that of the substitution reaction is 9.7 kcal/mol. The relatively low reaction barriers indicate a high thermodynamic probability for this photochemistry. This result is consistent with the experimental observation of strong Raman signals from *m*-^{3}(3-FBP·H_2O) and 3-BPOH. The structures presented in Figure 10 are the optimized geometries for the photosubstitution reaction of 3-FBP corresponding to the energy profile. In the first hydration step, the nucleophile attacked the carbon center at the *meta*-position, where the positive charge accumulates. The protonated species ^{3}(3-FBP·H^+) with a positive charge located at the *meta*-position is not stable in polar solvents (such as water here), giving a driving force for the hydration reaction to reduce the activation barrier by forming the more stable intermediate. The C−F bond elongated from 1.35 to 1.36 Å and finally to 1.41 Å in the reaction complex (RC), transition state (TS), and product complex (PC), respectively. In the meantime, the dihedral between the fluorine and the benzene ring dramatically changed from 175° to 166° and eventually to 127°. This reflects the strong influence of steric hindrance in the formation of the hydration species. In the next reaction step, the water molecule assisted the leaving of both the H and fluorine by the connection of hydrogen bonds, which is also an ESPT process. This suggests that water molecules act as a bridge or cluster to transfer the proton from the carbonyl oxygen to the substituted fluorine. The deprotonation and substitution reaction result in the formation of the 3-BPOH product when the separation of H and the cleavage of the C−F bond as well as the enhancement of O−H bonding occur simultaneously. Thus, the photosubstitution reaction is dramatically affected by a stereoelectronic effect and a steric effect. As is shown in Figure 32S, the simulations conducted for 3-ClBP and 3-BrBP demonstrated higher energy barriers than that of 3-FBP to generate the hydration species at the *meta*-position, which means it is more difficult to have the initial reaction at the *meta*-position, not to mention the subsequent substitution reaction. These computational results are consistent with our experimental observations that the photosubstitution reaction only took place for 3-FBP rather than for the 3-ClBP or 3-BrBP in 1.00 M $HClO_4$ CH_3CN/H_2O (1:1 by volume) solutions.

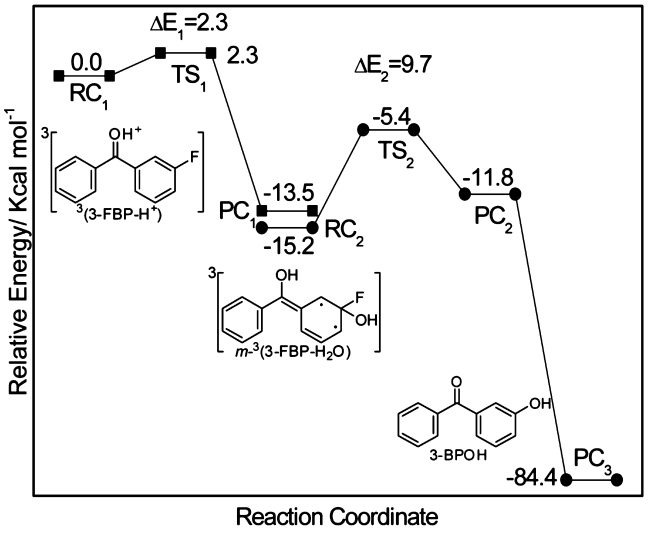

Figure 9. Reaction energy profile obtained from (U)B3LYP/6-311G** calculations for the photosubstitution reaction of 3-FBP with the assistance of two water molecules.

Based on the above discussion, we are able to predict the photophysical and photochemical properties of 4-ClBP and 4-BrBP in CH_3CN, 2-propanol, and CH_3CN/H_2O (1:1 by volume) solution would be the same as those of 3-FBP. The efficient ISC process from S_1 to T_1 and the characteristic Raman bands of triplet state and ketyl radical are obtained by fs-TA and TR^3 experiments in Figur 33S−37S, whereas we consider the photosubstitution reaction would not take place for 4-ClBP and 4-BrBP according to the substituent position and the type of substituted halogen. The *para*-position is not favored by the nucleophilic attack due to the steric crowding and the increase in the inductive effect from the substituted chlorine and bromine atoms. Since the nucleophile prefers to

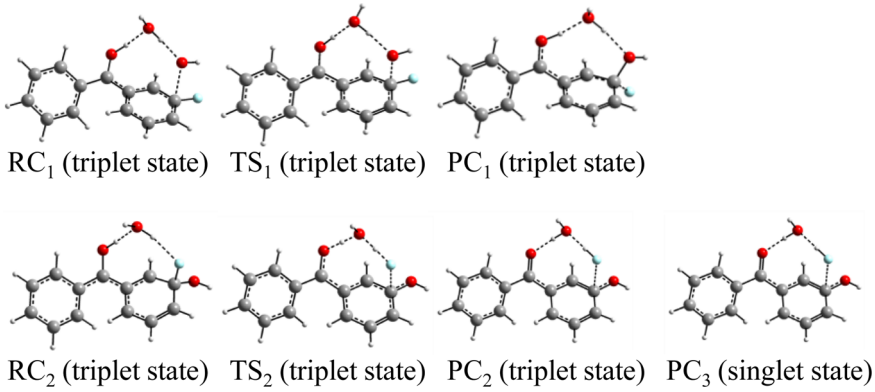

Figure 10. Optimized geometries of RC_n, TS_n, and PC_n obtained from UB3LYP/6-311G** calculations for the photosubstitution reaction of 3-FBP with the assistance of two water molecules. The activation barrier of the photohydration reaction on the *meta*-position is 2.3 kcal/mol. The activation barrier of the photosubstitution reaction is 9.7 kcal/mol.

DOI: 10.1021/acs.joc.5b01308
J. Org. Chem. 2015, 80, 9425−9436

attack at the *ortho*- or *meta*-positions while the halogen is substituted at a *para*-position, it is highly unlikely to produce an intermediate with the leaving group and the nucleophilic group attached to the same carbon. That means the probability of the photosubstitution reaction is almost nil, which is in good agreement with our results that no substituted product is detected for 4-ClBP and 4-BrBP in 1.00 M $HClO_4$ CH_3CN/H_2O (1:1 by volume) solution (Figures 38S and 39S).

The driving force behind this photosubstitution reaction might provide insight into several potential applications. Our results demonstrate how the water molecules and acid molecules greatly catalyzed the halogen elimination reactions. This behavior occurs via a simultaneous intramolecular proton transfer and separation of the leaving halogen through a water bridge or network. The intramolecular proton-transfer model of the excited state can also be utilized to understand other halogen elimination reactions in aqueous solution. The present work carries interesting implications for the mechanism of the aromatic substitution reaction. The work here in conjunction with the previous report demonstrates the special substituent position selectivity as well as the different activities of the substituted halogen in the excited state. It is feasible to design an appropriate modification on the existing target to control the efficiency of the photosubstitution reaction. Such photosubstitution reactions hold promising application as a new photochemical synthetic method and a novel way to adjust the photophysical and photochemical properties of photosensitive materials.

CONCLUSION

The photophysical and photochemical reactions of a series of halogen-substituted BPs (3-FBP, 3,3′-DFBP, 4-FBP, 3-ClBP, 4-ClBP, 3-BrBP, and 4-BrBP) are similar to the behavior of BP in CH_3CN, 2-propanol, and neutral water-containing solutions. However, in 1.00 M $HClO_4$ CH_3CN/H_2O (1:1 by volume) condition, 3-FBP underwent an efficient photosubstitution, which is shown in Scheme 1. The influences of the acidity, the substituent position, and the type of substituted halogen on this photosubstitution reaction were investigated, and several conclusions can be made. First, it is found that the photosubstitution reaction is acid-catalyzed and has a high efficiency in 1.00 M $HClO_4$ CH_3CN/H_2O (1:1 by volume) solution. Second, it is found that this photosubstitution reaction only took place at the *ortho*- or the *meta*-positions, where the attacking hydroxyl and the leaving group could attach to the same aliphatic carbon center. The nucleophile still preferred the *ortho*- and *meta*-positions when the fluorine substituted at a *para*-position, so no substituted product was detected for 4-FBP in 1.00 M $HClO_4$ CH_3CN/H_2O (1:1 by volume) solution. Thus, the photosubstitution reaction of 3-FBP could extend the phenomena of the *meta* effect in photochemistry. Third, the photosubstitution reaction occurred only if the substituted halogen is fluorine for the systems and conditions examined so far. The signal of 3-BPOH is absent in the ns-TR^3 spectra of either 3-ClBP or 3-BrBP under parallel conditions because the substituted chlorine and bromine led to more steric crowding and had a decrease in the electron-withdrawing inductive effect. Therefore, this two-step nucleophilic photosubstitution reaction is dramatically affected by both a stereoelectronic effect and possibly a steric effect.

Our recent time-resolved spectroscopy studies of *meta*-substituted derivatives point out that the special *meta* effect may not be restricted only to a singlet state.[28] This study of halogen-substituted BPs not only supports but also provides insight into the profound *meta* effect in aromatic carbonyl photochemistry. On the basis of the above discussions, it is predictable that the photosubstitution reaction would occur on 2-fluorobenzophenone but probably not (or much less efficiently) on 2-chlorobenzophenone or 2-bromobenzophenone. However, further investigation is needed to elucidate the actual extent of photosubstitution reactions of the *ortho*- compared to the *meta*-halogen-substituted BPs. One can expect that this new photochemical reaction mechanism for the halogen-substituted BP derivatives and the factors that influence the appearance and potential control of these reactions can be utilized for a variety of applications such as photochemical treatment for aromatic halogen hazards in the environment, photochemical defluoridation of drinking water, and photochemical halogen substituent modification for photosensitive materials in synthesis.

EXPERIMENTAL AND COMPUTATIONAL METHODS

A. Preparation of the Samples for the Experiments. 4-Fluorobenzophenone (4-FBP), 4-chlorobenzophenone (4-ClBP), 4-bromobenzophenone (4-BrBP), 3-fluorobenzophenone (3-FBP), 3-hydroxybenzophenone (3-BPOH), 3,3′-difluorobenzophenone (33′-DFBP), 3-chlorobenzophenone (3-ClBP), 3-bromobenzophenone (3-BrBP), 2-fluorobenzophenone (2-FBP), 2-chlorobenzophenone (2-ClBP), and 2-bromobenzophenone (2-BrBP) were commercial chemicals with 98% purity. Spectroscopic grade 2-propanol, acetonitrile (CH_3CN), and deionized water were used. Perchloric acid ($HClO_4$) was used to prepare the water-containing sample solutions with different concentrations. Without notification, all of the mixed water-containing solvents are a volumetric ratio. The highly acidic solution contains 1.00 M $HClO_4$ in CH_3CN/H_2O (1:1 by volume) mixed solution. The moderately acidic solution contains 0.10 M $HClO_4$ in CH_3CN/H_2O (1:1 by volume) mixed solution. The weakly acidic solution contains 0.01 M $HClO_4$ in CH_3CN/H_2O (1:1 by volume) mixed solution.

During the experiments, the sample solutions were flowing through a flowing cell where the pump laser beam and the probe laser beam were overlapped. The photochemical reactions were initiated by the pump pulse then the intermediates were detected by the probe pulse.

B. Femtosecond Transient Absorption (fs-TA) and Nanosecond Transient Absorption (ns-TA) Experiments. A regenerative amplified Ti:sapphire laser system together with an automated data acquisition system were used to carry out the femtosecond transient absorption (fs-TA) spectroscopy experiments.[28,29] Utilizing a CaF_2 crystal, around 5% of the amplified output (800 nm) was generated from the amplified laser system was used to produce a white-light continuum from 350 to 750 nm. This continuum was used as the probe pulse. The pump pulse used is a 266.6 nm laser beam, generated by the third harmonic of the fundamental 800 nm from the regenerative amplifier. The maximum temporal delay used for the optical stage is 3300 ps. The instrument response time was approximately 150 fs. During each temporal delay, the data should be averaged over 2 s. The generated probe light is split to two separate beams, one is sent to the sample, the other is directed going into a reference spectrometer where fluctuations in the probe beam intensity are detected. Fiber optics were coupled to a multichannel spectrometer connected to a CMOS sensor with a 1.5 nm intrinsic resolution. Data were acquired from a 40 mL of the sample solution flowing through a 2 mm path length cuvette. The degradation of the samples was monitored by utilizing UV absorption spectroscopic measurements during the data collection period. Old samples were replaced with fresh samples to avoid degradation from affecting the results. The data were recorded as three-dimensional wavelength−time−absorbance matrices. In order to have an equal number of photons absorbed under the same irradiating environment in each

DOI: 10.1021/acs.joc.5b01308
J. Org. Chem. 2015, 80, 9425−9436

sample, the absorbance at 266.6 nm of each sample solution was kept the same as 1. In order to show the spectral changes clearly, the spectra shown in this paper are partially selected from the experimental data.

Nanosecond transient absorption (ns-TA) experiment is conducted on an LP-920 Laser flash photolysis setup by Edinburgh Instruments.[28,29] The fourth harmonic of an Nd:YAG Q-switched laser is used as the pump pulse, giving a laser beam of wavelength 266.0 nm, while the probe pulse is given by a 450 W xenon lamp. The two laser beams are adjusted to pass into the sample at right angles to each other, both are focused onto a quartz cell 1 cm in size. During nanosecond experiments, the warm up time of lasers should be at least 1 h until the laser power is stable. The laser power is measured by the power meter and should be adjusted to the same value before conducting nanosecond experiments. At each time point, the signal is averaged 10 times to diminish the influence of laser power fluctuations. The pump beam excited the sample; after going through the sample, the analyzing probe beam goes directly into a monochromator/spectrograph. The transmitted probe light is then detected by an array detector to analyze the spectra at a given time or by a single detector to analyze the kinetic of a single wavelength. The transmission conversions are transformed into electrical signals by the detector, which are acquired by a CCD camera as an array detector or measured by an oscilloscope as the single detector. The changes in optical density are then interpreted in terms of changes in transmission properties. A Hamamatsu R928 photomultiplier is used to detect the signal separated from a symmetrical Czerny-Turner monochromator, which then proceeds to an analytical software on interfaced PC. All the ns-TA experiments are performed in air-saturated solutions and the sample solutions are prepared to have the same absorbance at the specified λ_{ex}. Therefore, the equal number of photons is irradiated under the same conditions for each sampling.

C. Nanosecond Time-Resolved Resonance Raman (ns-TR^3) Experiments. The ns-TR^3 experiments have been described in our previous studies,[10,28,29,38] and only a brief account is given here. The ns-TR^3 experiments used two Nd:YAG lasers to produce one pump laser beam and one probe laser beam, respectively. The former laser was used to provide a wavelength of 266.0 nm from the fourth harmonic of the Nd:YAG laser, while the latter laser was used to provide a wavelength of 319.9 nm using the hydrogen Raman-shifted third anti-Stokes line of the 532.0 nm second harmonic. The laser beams were adjusted to ensure both beams overlap spatially onto the flowing liquid sample. A time delay between the pump and probe lasers was introduced and controlled using a pulse delay generator. The sample was excited by the pump laser to initiate the photochemical reaction. The probe laser pulse, which arrives slightly after the pump laser pulse, probes the intermediate species produced by the photochemical reaction. The probe light is Raman-scattered by the intermediates, and the scattered light is directed to a liquid nitrogen cooled charge-coupled device (CCD) using a backscattering geometry. The CCD signal was read out onto a PC computer once every 10 s, and every 10 readouts was summed up to give one resonance Raman spectrum. The ns-TR^3 spectrum can then be determined by appropriately subtracting pump only and probe only resonance Raman spectra from a pump−probe spectrum at the time-delay used for the experiments. The Raman shifts were calibrated using CH_3CN, with an accuracy of around 5 cm^{-1}. Sample concentrations used in the ns-TR^3 experiments were $\sim 3 \times 10^{-3}$ M.

D. DFT Calculations. DFT computations using the (U)B3LYP/6-311G** level of theory were performed to obtain the vibrational wavenumbers and the optimized geometries of the proposed intermediates. The predicted Raman spectra were acquired by the G09 program suite that used the determination of the Raman intensities from the transition polarizabilities calculated by a numerical differentiation with an assumed zero excitation frequency (e.g., the Placzek approximation).[28,29] To predict the computed Raman spectra, a Lorentzian function with a 15 cm^{-1} bandwidth was used for the Raman vibrational frequencies and the relative intensities. When the calculated spectra were compared to the experimental results, a frequency scaling factor (0.974) was employed.[28,29] The optimized structures were obtained at the stationary states with no imaginary frequency modes. For the saddle point transition-state structures, one imaginary frequency for the reactive mode was attained. The proposed reaction steps were examined by simulating the structures of the reactant complexes (RC), product complexes (PC), and transition states (TS), which could be located by utilizing the Berny algorithm. The particular nature of the transition states was examined by analyzing the motion from the descriptions of the eigenvector combined with the imaginary frequency and intrinsic reaction coordinates were computed on the TSs to verify that every transition state structure connected the two corresponding minima structures for the RC and PC. All of the computations were performed using the Gaussian 09 program suite[40] on a computing cluster located at the University of Hong Kong.

■ ASSOCIATED CONTENT

Supporting Information

The Supporting Information is available free of charge on the ACS Publications website at DOI: 10.1021/acs.joc.5b01308.

Figures 1S−39S, Cartesian coordinates, and full Gaussian reference (PDF)

■ AUTHOR INFORMATION

Corresponding Authors

*E-mail: anini1984@163.com.

*E-mail: phillips@hku.hk.

Notes

The authors declare no competing financial interest.

■ ACKNOWLEDGMENTS

This work was supported by grants from the Research Grants Council of Hong Kong (HKU 17301815) to D.L.P. and the National Science Fundation of China (21503167). Partial support from the Grants Committee Areas of Excellence Scheme (AoE/P-03/08) and a Special Equipment Grant (SEG HKU/07) are also gratefully acknowledged.

■ REFERENCES

(1) Klán, P.; Šolomek, T.; Bochet, C. G.; Blanc, A.; Givens, R.; Rubina, M.; Popik, V.; Kostikov, A.; Wirz, J. *Chem. Rev.* **2013**, *113*, 119.

(2) Patterson, G. H.; Lippincott-Schwartz, J. *Science* **2002**, *297*, 1873.

(3) Sasse, A.; Ligneau, X.; Sadek, B.; Elz, S.; Pertz, H. H.; Ganellin, C. R.; Arrang, J.-M.; Schwartz, J.-C.; Schunack, W.; Stark, H. *Arch. Pharm.* **2001**, *334*, 45.

(4) Mésange, F.; Sebbar, M.; Capdevielle, J.; Guillemot, J.-C.; Ferrara, P.; Bayard, F.; Poirot, M.; Faye, J.-C. *Bioconjugate Chem.* **2002**, *13*, 766.

(5) Heine, H. G.; Rosenkranz, H. J.; Rudolph, H. *Angew. Chem., Int. Ed. Engl.* **1972**, *11*, 974.

(6) Levin, P. P.; Efremkin, A. F.; Sultimova, N. B.; Kasparov, V. V.; Khudyakov, I. V. *Photochem. Photobiol.* **2014**, *90*, 369.

(7) Xiao, P.; Dumur, F.; Graff, B.; Gigmes, D.; Fouassier, J. P.; Lalevée, J. *Macromolecules* **2013**, *46*, 7661.

(8) Boscá, F.; Miranda, M. A. *J. Photochem. Photobiol., B* **1998**, *43*, 1.

(9) Cai, X.; Sakamoto, M.; Fujitsuka, M.; Majima, T. *Chem. - Eur. J.* **2005**, *11*, 6471.

(10) Encinas, S.; Belmadoui, N.; Climent, M. J.; Gil, S.; Miranda, M. A. *Chem. Res. Toxicol.* **2004**, *17*, 857.

(11) Peters, K. S.; Cashin, A.; Timbers, P. *J. Am. Chem. Soc.* **2000**, *122*, 107.

(12) Sakamoto, M.; Cai, X.; Fujitsuka, M.; Majima, T. *Chem. - Eur. J.* **2006**, *12*, 1610.

(13) Porter, G.; Tchir, M. F. *J. Chem. Soc. A* **1971**, 3772.

(14) Nadjo, L.; Sevéant, J. M. *J. Electroanal. Chem. Interfacial Electrochem.* **1971**, *30*, 41.

DOI: 10.1021/acs.joc.5b01308
J. Org. Chem. 2015, 80, 9425−9436

(15) Mahalakshmi, G.; Balachandran, V. *Spectrochim. Acta, Part A* **2014**, *124*, 328.
(16) Porter, G.; Wilkinson, F. *Trans. Faraday Soc.* **1961**, *57*, 1686.
(17) Pews, R. G.; Tsuno, Y.; Taft, R. W. *J. Am. Chem. Soc.* **1967**, *89*, 2391.
(18) Peters, K. S.; Cashin, A. *J. Phys. Chem. A* **2000**, *104*, 4833.
(19) Wolf, M. W.; Legg, K. D.; Brown, R. E.; Singer, L. A.; Parks, J. H. *J. Am. Chem. Soc.* **1975**, *97*, 4490.
(20) Sakamoto, M.; Cai, X.; Hara, M.; Tojo, S.; Fujitsuka, M.; Majima, T. *J. Phys. Chem. A* **2004**, *108*, 8147.
(21) Bhattacharyya, K.; Das, P. K. *J. Phys. Chem.* **1986**, *90*, 3987.
(22) Moriconi, E. J.; O'Connor, W. F.; Forbes, W. F. *J. Am. Chem. Soc.* **1962**, *84*, 3928.
(23) Giorgianni, S.; Passerini, A.; Gambi, A.; Ghersetti, S.; Spunta, G. *Spectrosc. Lett.* **1980**, *13*, 445.
(24) Passerini, A.; Giorgianni, S.; Gambi, A.; Ghersetti, S.; Spunta, G. *Spectrosc. Lett.* **1980**, *13*, 729.
(25) Fukuda, E. K.; McIver, R. T. *J. Am. Chem. Soc.* **1985**, *107*, 2291.
(26) Li, W.; Xue, J.; Cheng, S. C.; Du, Y.; Phillips, D. L. *J. Raman Spectrosc.* **2012**, *43*, 774.
(27) Ramseier, M.; Senn, P.; Wirz, J. *J. Phys. Chem. A* **2003**, *107*, 3305.
(28) Ma, J.; Su, T.; Li, M.-D.; Du, W.; Huang, J.; Guan, X.; Phillips, D. L. *J. Am. Chem. Soc.* **2012**, *134*, 14858.
(29) Ma, J.; Su, T.; Li, M.-D.; Zhang, X.; Huang, J.; Phillips, D. L. *J. Org. Chem.* **2013**, *78*, 4867.
(30) Burnett, J. F.; Zahler, R. E. *Chem. Rev.* **1951**, *49*, 273.
(31) Cornelisse, J.; Havinga, E. *Chem. Rev.* **1975**, *75*, 353.
(32) Buchanan, G. W.; Montaudo, G.; Finocchiaro, P. *Can. J. Chem.* **1973**, *51*, 1053.
(33) Kong, F.-F.; Zhai, B.-C.; Song, Q.-H. *Photochemical & Photobiological Sciences* **2008**, *7*, 1332.
(34) Li, M.-D.; Yeung, C. S.; Guan, X.; Ma, J.; Li, W.; Ma, C.; Phillips, D. L. *Chem. - Eur. J.* **2011**, *17*, 10935.
(35) Huang, J.; Yeung, C. S.; Ma, J.; Gayner, E. R.; Phillips, D. L. *J. Phys. Chem. A* **2014**, *118*, 1557.
(36) Kong, F.-F.; Wang, J.-B.; Song, Q.-H. *Beilstein J. Org. Chem.* **2011**, *7*, 113.
(37) Du, Y.; Ma, C.; Kwok, W. M.; Xue, J.; Phillips, D. L. *J. Org. Chem.* **2007**, *72*, 7148.
(38) Du, Y.; Xue, J.; Li, M.; Phillips, D. L. *J. Phys. Chem. A* **2009**, *113*, 3344.
(39) Klán, P.; Wirz, J. In *Photochemistry of Organic Compounds*; John Wiley & Sons, Ltd.: New York, 2009; p 137.
(40) Frisch, M. J.; Trucks, G. W.; Schlegel, H. B.; Scuseria, G. E.; Robb, M. A.; Cheeseman, J. R.; Scalmani, G.; Barone, V.; Mennucci, B.; Petersson, G. A.; Nakatsuji, H.; Caricato, M.; Li, X.; Hratchian, H. P.; Izmaylov, A. F.; Bloino, J.; Zheng, G.; Sonnenberg, J. L.; Hada, M.; Ehara, M.; Toyota, K.; Fukuda, R.; Hasegawa, J.; Ishida, M.; Nakajima, T.; Honda, Y.; Kitao, O.; Nakai, H.; Vreven, T.; Montgomery, J. A., Jr.; Peralta, J. E.; Ogliaro, F.; Bearpark, M. J.; Heyd, J.; Brothers, E. N.; Kudin, K. N.; Staroverov, V. N.; Kobayashi, R.; Normand, J.; Raghavachari, K.; Rendell, A. P.; Burant, J. C.; Iyengar, S. S.; Tomasi, J.; Cossi, M.; Rega, N.; Millam, N. J.; Klene, M.; Knox, J. E.; Cross, J. B.; Bakken, V.; Adamo, C.; Jaramillo, J.; Gomperts, R.; Stratmann, R. E.; Yazyev, O.; Austin, A. J.; Cammi, R.; Pomelli, C.; Ochterski, J. W.; Martin, R. L.; Morokuma, K.; Zakrzewski, V. G.; Voth, G. A.; Salvador, P.; Dannenberg, J. J.; Dapprich, S.; Daniels, A. D.; Farkas, Ö.; Foresman, J. B.; Ortiz, J. V.; Cioslowski, J.; Fox, D. J. Gaussian, Inc.: Wallingford, CT, 2009.

DOI: 10.1021/acs.joc.5b01308
J. Org. Chem. 2015, 80, 9425−9436